Seismic testing and performance analysis of "JETPACS" structure protected by pressurized fluid viscous damped braces

Seismic testing and performance analysis of "JETPACS" structure protected by pressurized fluid viscous damped braces

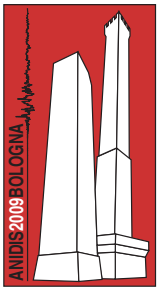

Stefano Sorace, Fabio Fadi
Dipartimento di Ingegneria Civile e Architettura, Università di Udine. Via delle Scienze 206, 33100 Udine.

Gloria Terenzi
Dipartimento di Ingegneria Civile e Ambientale, Università di Firenze. Via di S. Marta 3, 50139 Firenze.

Keywords: Seismic testing, Shaking table, Seismic retrofit, Fluid viscous dissipaters, Dissipative braces

ABSTRACT
Selected results of the shaking table testing campaign and relevant interpretation analyses carried out, within the Research Project No. 7 of DPC-ReLUIS Executive Project 2005-2008, on the JETPACS steel structure equipped with dissipative braces incorporating Jarret pressurized fluid viscous spring-dampers, are presented in this paper. The characteristics of the test structure tested at the Structural and Material Testing Laboratory of the University of Basilicata, and the finite element model generated to perform the analytical enquiry, are initially described. Calibration of model parameters based on the results of the dynamic identification tests developed on the bare and protected structure, as well as on the spring-dampers, is then discussed. The design of the fluid viscous dissipaters adopted for this installation is also outlined. The set of 35 tests carried out is recapitulated, and the results of the most significant experiments, and the corresponding analytical simulations, are presented in detail. A formal performance-based assessment analysis, developed for the original and protected structure by combining test data and the results of a supplementary numerical enquiry developed by the finite element models of both layouts, is finally illustrated.

1 INTRODUCTION

The dissipative bracing system incorporating Jarret pressurized fluid viscous spring-dampers as passive protective devices (Jarret SL 2008), examined in this study, was conceived and set up in previous research Projects (Sorace and Terenzi 2003, 2008, 2009). Special design and analytical modelling criteria were also proposed within these Projects. Furthermore, pseudodynamic testing campaigns were developed on large-scale and full-scale steel and reinforced concrete structures, always showing high performance capacities of the protection system (Sorace and Terenzi 2003, 2004, 2008, Molina et al. 2004).

As a natural completion of these activities, a first real-time seismic verification programme was developed on the system thanks to the participation of the Unit of Udine University to the mutual experimental campaign carried out, within the DPC-ReLUIS Executive Project 2005-2008, by the shaking table apparatus of the Material and Structural Testing Laboratory of the University of Basilicata. This campaign involved also several other Units taking part to Research Project No. 7 (Dolce et al. 2008).

As discussed in the next sections, this new experimental research confirmed further the effectiveness of this special dissipative bracing technology in passive seismic protection of frame structures. This was also highlighted by a formal performance assessment analysis in original and retrofitted conditions, elaborated by combining the experimental data and the results of the numerical analyses carried out by the finite element model of test structure.

2 DESCRIPTION OF TEST STRUCTURE

The test structure is a 2/3-scale model of a one-span, two-story double frame, with 4 m-long spans and 2 m-high stories. The two constituting frames are placed at a mutual distance of 3 m. A photographic view and the geometrical

characteristics of the structure in protected conditions are shown in Figures 1 and 2. The floors are made of HI-bond corrugated steel sheets, with upper 100 mm-thick reinforced concrete slabs. Columns and beams are in HEB 140 and IPE 180 Italian profiles, respectively. Beam-to-column joints are welded and stiffened by horizontal plates crossing the panel zones of columns. The structure is anchored at its base to a horizontal frame made of HEB 220 steel beams, joined to the dynamic actuator of the testing apparatus. HEA 100 inverse chevron braces are installed as unified supporting elements for the different types of dissipaters to be mounted in the various stages of the experimental programme (Dolce et al. 2008). All the structural members are made of Fe360 grade steel, with the following characteristics: Young modulus E=206000 MPa, yielding stress $f_y \geq 235$ MPa, and ultimate stress $f_u \geq 360$ MPa.

Figure 1. View of test structure in protected configuration.

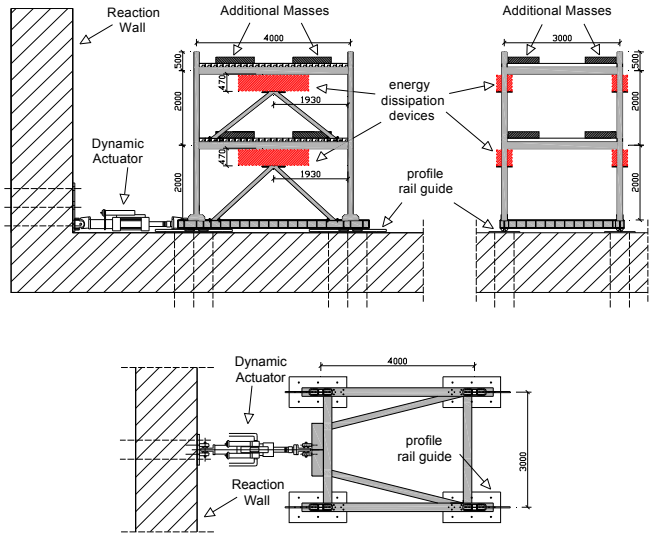

Figure 2. Test structure: front, side and plan views.

3 FINITE ELEMENT MODEL OF ORIGINAL STRUCTURE

The finite element model of the original structure was generated by the commercial calculus code SAP2000NL (CSI 2008), and calibrated on the results of the dynamic identification tests carried out at the initial stage of the experimental programme. Different excitation sources were considered to obtain natural frequencies, modal shapes, and damping values. Three different mass configurations were examined: Basic (B), represented by the bare structure; Additional Eccentric (AE), obtained by placing 2 additional concrete blocks on one side only, at each floor; Additional Symmetric (AS), with 4 blocks arranged in a symmetrical layout. The latter configuration, displayed in Figure 2, was also adopted throughout the shaking table campaign in protected conditions, so as to increase the global weight of the structure and thus the seismic forces produced by the input ground motions. Calibration of the analytical model was performed against the results of dynamic identification tests carried out for all the three mass configurations. For sake of brevity, only the data referred to the AS layout are reported in Table 1 below.

Table 1. Test structure weights.

Elements	Weights (kN)
Steel frame	11.1
2 concrete slabs (steel sheets included)	53.2
8 concrete blocks	27.2
Total weights	91.5

Based on the weight values in Table 1, a lumped-mass finite element model was generated, by assigning a translational mass of 1.16 kN/(m/s^2) to each one of the eight beam-to-column joints for both directions in plan, and imposing a rigid floor constraint at each story. Additional negative polar moments of inertia with respect to the vertical axis Z were then assigned to the eight joints, so as to compensate for the overestimation of the rotational inertia of floors deriving from the lumped-mass scheme. The value of each additional polar moment of inertia computed for the AS configuration is: I_a=-1.29 kNm^2/(m/s^2).

The natural periods of the model in AS configuration are compared in Table 2 with the corresponding values derived from the dynamic identification tests (Dolce et al. 2008). Total

correlation between analytical and experimental values along the main axis in plan, X (which coincides with the uniaxial shaking table testing direction), and negligible differences for the translational modes along Y and the torsional modes around Z (all below 0.01 s), are observed.

Table 2. Experimental and analytical vibration periods of test structure.

Mode	Direction	Test structure Period (s)	Model Period (s)
1	Y	0.35	0.34
2	X	0.28	0.28
3	Z	0.20	0.19
4	Y	0.12	0.11
5	X	0.08	0.08
6	Z	0.06	0.06

4 CHARACTERISTICS OF FLUID VISCOUS DEVICES AND SYSTEM INSTALLATION

The scheme of installation of Jarret spring-dampers on test structure resembles, with some adjustments, the general layout conceived for this technology (Sorace and Terenzi 2008, 2009). Therein, a pair of interfaced devices are placed, in parallel with the floor-beam axis, at the tip end of each couple of supporting steel braces. A half-stroke initial position is imposed to the pistons of both spring-dampers, so as to obtain symmetrical tension-compression response cycles, starting from a compressive-only response of the single devices. This position is obtained by introducing a pair of threaded steel bars through a central bored plate orthogonal to the interfacing plate of the two devices; the bars are connected at both ends to other two bored plates, screwed into the external casing of the spring-dampers. The axial force required to drive the pistons at their half-strokes is applied to the steel bars by a torque wrench, by acting on the nuts in contact with the two plates screwed on the devices. The terminal section of the external casing of each FV device is encapsulated into a steel "cap" hinged to two vertical trapezoidal plates welded to the upper horizontal plate of the assembly, which is fixed to the lower face of the floor beam. The caps constrain the spring-dampers to move with the same displacement as the floor beam.

As shown by the photographic image in Figure 4, the two main adjustments required for the installation on the JETPACS structure consist in: a much larger mutual distance of the dissipaters, determined by the asymmetrical vertical plate placed between the pistons, introduced to accommodate the greater devices incorporated in the other protection systems to be tested in this Project; and a single-side connection to the floor beam, since in most of the other systems only one damper per floor (on each side) had to be mounted.

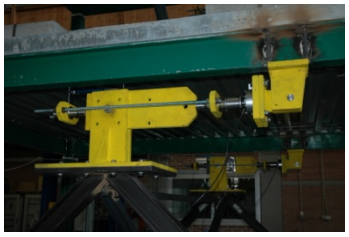

Figure 3. View of a fluid viscous damper assembly installed on test structure.

The geometry of the finite element model reproducing the device assembly installed on test structure is sketched in Figure 4, in superimposition to the design drawing of this connection. In this model, each steel bar is simulated by a single truss element connecting the farthest ends of the fluid viscous dampers, highlighted by joints A and B in Figure 4. This allowed avoiding any connection to the intermediate elements overlapped by the connection truss. Within this finite element assembly, the dampers are modelled according to the general scheme presented in (Sorace and Terenzi 2008), recalled in the next section.

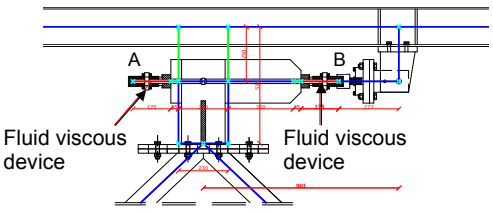

Figure 4. Drawing of a FV spring-damper–braces–beam connection in test structure.

The $F_d(t)$ damping and $F_{ne}(t)$ non-linear elastic reaction forces of this class of devices can be expressed analytically as follows (Peckan et al. 1995, Sorace and Terenzi 2001):

$$F_d(t) = c\,\mathrm{sgn}(\dot{x}(t))\left|\dot{x}(t)\right|^{\alpha} \tag{1}$$

$$F_{ne}(t) = k_2 x(t) + \frac{(k_1 - k_2)\,x(t)}{\left[1 + \left|\frac{k_1 x(t)}{F_0}\right|^{R}\right]^{1/R}} \tag{2}$$

where c = damping coefficient; sgn(·) = signum function; |·| = absolute value; α = fractional exponent, ranging from 0.1 to 0.2; F_0 = static pressurization pre-load; k_1, k_2 = stiffness of the response branches situated below and beyond F_0; and R = integer exponent, set as equal to 5 (Sorace and Terenzi 2001). An effective simulation of the response of fluid viscous spring-dampers is obtained by combining Eqs. (1) and (2), which are also incorporated in commercial structural analysis programs, such as the SAP2000NL code used in these analyses. In addition to a dashpot and a spring, the reaction forces of which are expressed by Eqs. (1) and (2), the computational model of a fluid viscous device is completed by a "gap" and a "hook" assembled in parallel, aimed at disconnecting the device when stressed in tension, and at stopping it when the maximum stroke is reached, respectively (Sorace and Terenzi 2008). Within this model, displayed in Figure 5, the static pre-load F_0 is imposed as an internal force to a bar linking the four elements to the interfaced structural elements.

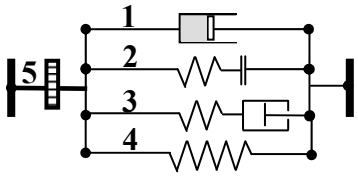

Figure 5. Computational model of a pressurized fluid viscous spring-damper (1. non-linear dashpot; 2. gap; 3. hook; 4. non-linear spring; 5. internal force equal to F_0).

As highlighted by Eqs. (1) and (2), the behaviour of a pressurized fluid viscous spring-damper is governed by parameters c, α, k_1, k_2 and F_0. Among these, α is directly assigned by the manufacturer within the range [0.1, 0.2]; k_1 defines the nearly rigid first elastic branch, and is set as equal to 15 k_2; F_0 is also fixed during manufacturing to obtain the required level of pressurization of the fluid. As regards elastic stiffness k_2 of the second branch, unlike other applications where an actual spring-damper function is required (such as base isolation, Sorace and Terenzi 2001), it is not an explicit parameter when fluid viscous devices are installed in a damped bracing system. Indeed, the choice of spring-dampers instead of pure dampers is only owed to the fact that even the smallest pure silicone dampers currently available are generally too large to be used in dissipative braces incorporated in building structures. Therefore, for this type of application, the damping coefficient c is the only actual design parameter. Once c has been fixed, the device providing this value is automatically located in the manufacturer's catalogue through its nominal energy dissipation capacity E_n, and k_2 becomes only an additional mechanical characteristic, like α, k_1 and F_0, and not a design parameter.

The design values of c for this application were fixed by the iterative procedure proposed in (Sorace and Terenzi 2008). It consists in assigning FV devices the capability of dissipating a prefixed fraction of the total seismic input energy computed for the finite element model of the structure on each story, as summed up in the following expression:

$$E_{Dj} = \beta_j E_{ij} \tag{3}$$

where β_j is the energy ratio for the jth story, E_{Dj} is the energy dissipated in the jth story and E_{ij} is the "absolute" input energy (Uang and Bertero 1988) of the jth story. Energy dissipated in the jth story is defined as (Sorace and Terenzi 2008):

$$E_{Dj} = \int_o^{t_c} c_j \left|\dot{v}_j\right|^{\alpha} \mathrm{sgn}\left(\dot{v}_j\right) \dot{v}_j dt \tag{4}$$

where t_c is the instant at which the calculation is carried out, c_j is the global damping coefficient at the jth story, and $\dot{v}_j$ is the relative velocity of the jth story. Finally, the absolute input energy at jth story is defined by the following expression:

$$E_{Ij} = \int_o^{t_c} m_j \ddot{v}_{tj} dv_g \tag{5}$$

where m_j is the mass associated to the jth story, $\ddot{v}_{tj}$ is the absolute acceleration of the jth story, and v_g is the ground displacement. The process starts from an initial evaluation of the input energy at the jth story E_{Ij}^{wd}, for the finite element model already including the braces and the spring component of FV spring-dampers, but without their damper component (i.e., the dashpot element in Figure 5).

The protection system was designed according to IMPW (2005) for Seismic Zone 1 (peak ground motion – PGA – equal to 0.35g for rigid

soil) and Soil Class B (soil factor equal to 1.25). The resulting PGA is 0.44 g (0.35 g × 1.25). The preliminary evaluation of c coefficients was carried out by referring to an artificial accelerogram consistent with the elastic response spectrum of IMPW (2005), and the most demanding real ground motion that was planned to be used as input in the shaking table tests (named 535ya, scaled at 100% of the original PGA). Application of the preliminary design procedure, illustrated in Sorace et al. (2009), led to the following global damping coefficient demands for the first and second story, respectively: c_{1st}=52 kN(s/m)$^{\alpha}$, c_{2st}=22 kN(s/m)$^{\alpha}$. These values were particularly determined by the 535ya motion. The smallest four plus four Jarret spring-dampers capable of providing the c_{1st} and c_{2st} preliminary design values are BC1DN, and BC1BN type, respectively (Jarret SL 2008), featured by the following mechanical parameters: k_2=730 kN/m, c=14 kN(s/m)$^{\alpha}$ – BC1DN; k_2=550 kN/m, c=6 kN(s/m)$^{\alpha}$ – BC1BN, with α=0.2 in both cases.

5 FINITE ELEMENT MODEL OF PROTECTED STRUCTURE

A global view of the finite element model of test structure in protected conditions is drawn in Figure 6. The model includes two special non-rigid connections, introduced to improve the correlation of the analytical response to the experimental one. The first connection, also illustrated in Figure 6, consists of a gap and a hook elements in series with the device assembly, aimed at reproducing the slippage of the bolted joint with respect to the reaction plate linked to the floor beam. The openings of the two nonlinear elements were calibrated on each test, to best match the experimental behaviour (Sorace et al. 2009).

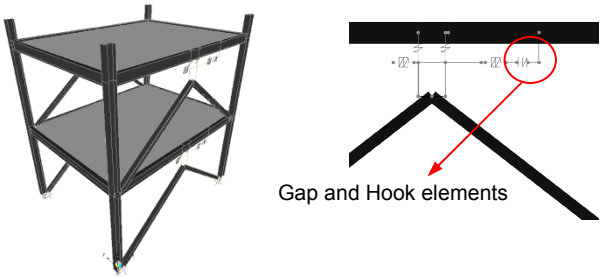

Figure 6. Finite element model of protected structure, and additional assembly implemented to simulate the slippage of the bolted joint to the vertical plate linked to the floor beam.

The second non-rigid connection is represented by a rotational elastic spring placed at the base of each column (with rotational degree-of-freedom orthogonal to the direction of excitation), which simulates the flexibility of columns feet highlighted by the seismic tests (Figure 7). The average spring stiffness derived from the experimental results is 8000 kNm/rad. Incorporation of the elastic springs allowed compensating the greater peak displacements obtained from tests, as compared to the analytical values produced by the model with fixed base columns (with differences up to 15%). Moreover, joint flexibility is very important to effectively reproduce the experimental response at the lowest levels of excitation.

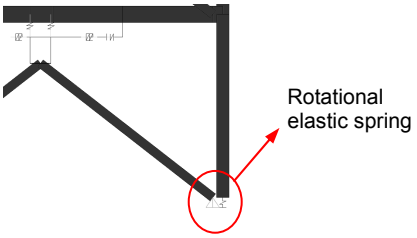

Figure 7. Rotational elastic springs introduced at the base of columns.

6 TEST RESULTS AND RELEVANT ANALYTICAL SIMULATIONS

The experimental programme was articulated in 33 seismic tests carried out by a set of 9 input ground motions, scaled to various amplitudes, plus an initial and a final characterisation tests developed by a random base excitation (Table 3). Among the 9 seismic motions, 7 are natural records (identified by labels S1 to S7) selected from the European Strong Motions Database, whose scaling factors were suggested in Iervolino et al. (2007). The mean spectrum of these records fits with reasonable approximation the design spectrum of IMPW (2005). The two remaining input motions are artificial accelerograms generated from the same response spectrum (S8 and S9). In the experimental applications, as well as in the numerical simulation analyses, all the accelerograms were scaled down in time by a factor $(1.5)^{1/2}$, to ensure consistency with the geometrical scale of test structure.

Three ground motions, namely S1 (1228xa), S2 (196xa) and S3 (535ya), were scaled at different amplitudes, with PGA fractions ranging from 10% to 150%, and intermediate fractions of 25%, 50%, 75%, 100%, and 125%. The mean

spectrum of these records scaled at 100% of PGA fits the response spectrum of IMPW (2005) with even better approximation than the spectrum computed for all the seven natural records does. The remaining four natural motions and the two artificial signals were applied at 100% and 125% of their original amplitudes.

Table 3. Shaking table tests performed.

Test	Test acronym
1	RND @ PGA 0.05g
2	S1 @ PGA 10%
3	S2 @ PGA 10%
4	S3 @ PGA 10%
5	S1 @ PGA 25%
6	S2 @ PGA 25%
7	S3 @ PGA 25%
8	S1 @ PGA 50%
9	S2 @ PGA 50%
10	S3 @ PGA 50%
11	S1 @ PGA 75%
12	S2 @ PGA 75%
13	S3 @ PGA 75%
14	S1 @ PGA 100%
15	S2 @ PGA 100%
16	S3 @ PGA 100%
17	S1 @ PGA 125%
18	S2 @ PGA 125%
19	S3 @ PGA 125%
20	S1 @ PGA 150%
21	S2 @ PGA 150%
22	S3 @ PGA 150%
23	S4 @ PGA 100%
24	S5 @ PGA 100%
25	S6 @ PGA 100%
26	S7 @ PGA 100%
27	S8 @ PGA 100%
28	S9 @ PGA 100%
29	S4 @ PGA 125%
30	S5 @ PGA 125%
31	S6 @ PGA 125%
32	S7 @ PGA 125%
33	S8 @ PGA 125%
34	S9 @ PGA 125%
35	RND@PGA 0.05g

Legend:
S1=natural–1228xa; S2=natural–196xa; S3=natural–535ya; S4=natural–187xa; S5=natural–291ya; S6=natural–4673ya; S7=natural–4677ya; S8=artificial 1; S9=artificial 2; RND = random.

Experimental results are reported in Table 4 through 7 and compared with the results of relevant numerical simulation analyses, for eight of the most demanding tests, i.e., those labelled with numbers 14, 15, 16, 20, 21, 22, 23 and 34 in Table 3. The following peak response quantities: story drift, interstory drift ratio, damper displacement, and brace force, are particularly recapitulated in Tables 4 through 7.

Table 4. Peak story drift: comparison of experimental and numerical results.

		Peak story drift (mm)			
		Story 1		Story 2	
Test	Ground motion	Exp.	Num.	Exp.	Num.
14	S1@PGA100%	1.9	2.2	4.4	4.0
15	S2@PGA100%	4.2	4.0	8.3	8.6
16	S3@PGA100%	7.2	6.5	13.9	12.9
20	S1@PGA150%	3.6	4.0	7.1	7.4
21	S2@PGA150%	7.2	6.6	13.9	14
22	S3@PGA150%	12.3	11.9	23.6	21.6
23	S4@PGA100%	6.9	7.1	13.9	13.1
34	S9@PGA125%	5.7	5.0	11.1	9.3

Table 5. Peak interstory drift ratio: comparison of experimental and numerical results.

		Peak interstory drift ratio (%)			
		Story 1		Story 2	
Test	Ground motion	Exp.	Num.	Exp.	Num.
14	S1@PGA100%	0.09	0.11	0.12	0.09
15	S2@PGA100%	0.21	0.20	0.18	0.23
16	S3@PGA100%	0.36	0.33	0.36	0.32
20	S1@PGA150%	0.18	0.20	0.14	0.17
21	S2@PGA150%	0.36	0.33	0.30	0.37
22	S3@PGA150%	0.62	0.59	0.57	0.48
23	S4@PGA100%	0.34	0.35	0.30	0.30
34	S9@PGA125%	0.29	0.25	0.27	0.22

Table 6. Peak damper displacement: comparison of experimental and numerical results.

		Peak damper displacement (mm)			
		Story 1		Story 2	
Test	Ground motion	Exp.	Num.	Exp.	Num.
14	S1@PGA100%	1.2	1.4	1.8	1.4
15	S2@PGA100%	3.4	3.4	3.5	4.0
16	S3@PGA100%	5.8	5.8	6.1	5.5
20	S1@PGA150%	2.5	2.5	2.8	2.6
21	S2@PGA150%	6.2	6.2	6.2	6.0
22	S3@PGA150%	11.5	11.2	9.4	9.0
23	S4@PGA100%	5.9	6.1	6.2	5.4
34	S9@PGA125%	4.0	4.0	4.7	3.9

Table 7. Peak brace force: comparison of experimental and numerical results.

		Peak brace force (kN)			
		Story 1		Story 2	
Test	Ground motion	Exp.	Num.	Exp.	Num.
14	S1@PGA100%	14	17	9	11
15	S2@PGA100%	23	23	14	15
16	S3@PGA100%	29	28	19	20
20	S1@PGA150%	18	20	11	12
21	S2@PGA150%	28	29	20	20
22	S3@PGA150%	37	40	38	43
23	S4@PGA100%	26	27	16	18
34	S9@PGA125%	25	23	15	16

As way of example, the results of tests performed with S3-535ya ground motion scaled at 150% and S9 accelerogram scaled at 125%, and relevant numerical simulations, are plotted in

Figures 8 and 9 in terms of first and second story displacement time-histories, second story damper force-displacement hysteresis loops, and energy time-histories. The first three diagrams are referred to one of the two constituting frames (named "west" side). The results are practically identical for the other frame ("east" side).

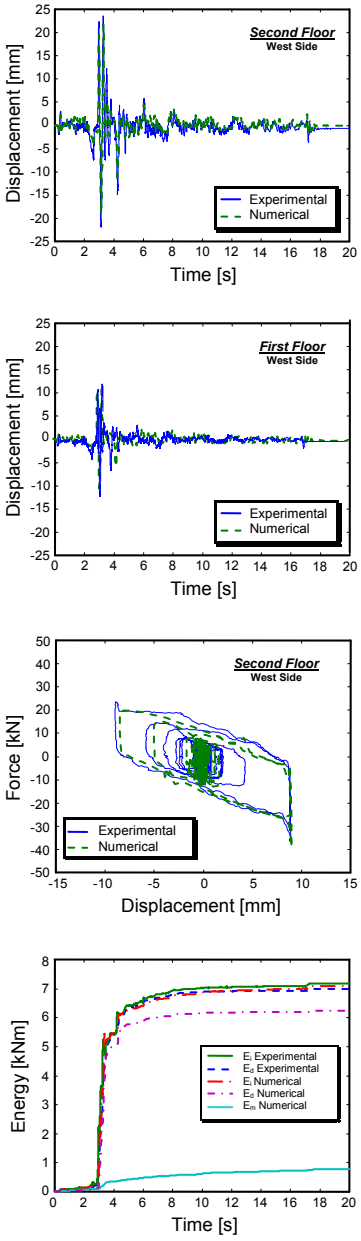

Figure 8. Comparison of experimental and numerical response to S3-535ya ground motion scaled at 150%.

The following remarks can be drawn from data reported in Tables 4 through 7.

1. Numerical analyses satisfactorily reproduce test results. In several cases numerical predictions are slightly non conservative, with maximum differences on displacements limited within 10%. The natural ground motion S3-535ya is the most demanding input at 100% and 150% scaled PGAs.

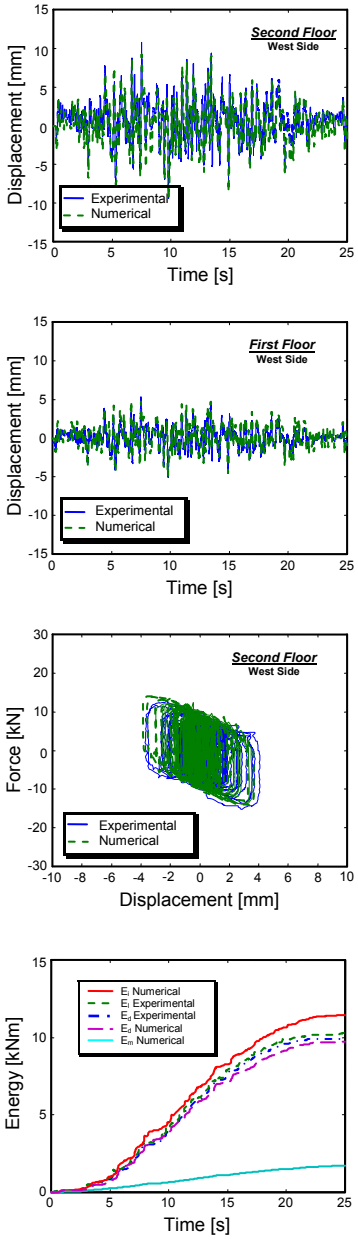

Figure 9. Comparison of experimental and numerical response to S9 ground motion scaled at 125%.

2. The peak interstory drift ratio induced by S3-535ya motion is equal to 0.36% for both floors, at 100% of PGA, and 0.62% for first floor and 0.57% for second floor, at 150% of PGA. All these values are below the drift limit formulated for steel structures by FEMA 356 (2000) for the immediate occupancy structural performance level. By considering that the earthquake levels imposed in these tests with the S3-535ya accelerogram are neatly beyond the amplitude of a basic design earthquake (test at 100% of PGA), and a maximum considered earthquake (test at 150% of PGA), the response in terms of drift ratios underlines an excellent performance of the protection system, as also discussed in section 3.

3. The design choice of dampers causes to obtain rather similar peak interstory drifts at both stories. This confirms the effectiveness of the experience-based assumption of a damping demand on second story equal to around 40% of the demand on first story, for two-story steel frame structures (Sorace and Terenzi 2008).
4. All peak damper displacements are below their net stroke, except for dampers at the second story in test 22 (S3-535ya input motion at 150% of PGA – third graph in Figure 8). However, the stroke is reached only in two instants, which does not produce any damage of the protection system and the frame members (these instantaneous "touches" are not practically caught by the structure).
5. The very low brace forces obtained also in the most demanding tests could have been absorbed by considerably smaller profiles than the ones installed on test structure. It is reminded here that these profiles were designed for the other protection systems to be installed in the subsequent stages of the experimental programme, characterised by greater dissipaters, and proportionately larger forces on braces.

Observation of graphs in Figures 8 and 9 prompt the following additional comments.

1. Comparison in terms of story displacements shows a good agreement between test results and numerical simulations, especially in correspondence with the peak response phases. The simulation of experiments at the lowest levels of excitation was generally more challenging. This is mainly due to the slippage effects in connections, which can be only roughly modelled for relatively low input actions (Sorace et al. 2009).
2. Comparison of hysteresis loops shows jagged curves from tests. This is mainly due to instrumental accuracy. At the same time, analytical loops show some noticeable spikes, as a consequence of the contacts that occur in gap and hook elements in certain instants of numerical response. These contacts produce a sudden increase of velocity, with the effect of transiently increasing the damping force, although with no practical influence on the damped energy balance.
3. Experimental and numerical energy time-histories are in good agreement too (E_i, E_d, E_m=input, damped, and modal energies), as a consequence of the global satisfactory correlation of test and analytical data. However, non negligible differences come out for some tests in terms of input energy (with up to 15% under- or overestimations of the experimental energy, in the numerical analyses). This is essentially due to the uncertainties in the computation of numerical modal damping energy, which can only be approximately estimated on the basis of the experimental response.

7 PERFORMANCE-BASED EVALUATION ANALYSIS OF ORIGINAL AND PROTECTED STRUCTURE

A final performance-based evaluation analysis was carried out on test structure in original and retrofitted conditions, to formally assess the enhancement of seismic response capacities produced by the incorporation of the dissipative bracing system. Supplementary numerical analyses were developed by introducing plastic hinges within the finite element model of the structure, and subjecting it to the same ground motions used as inputs in the shaking table tests. The benefits of the dissipative system were evaluated by: a) comparing the responses in original and protected conditions; and b) assessing both responses against the performance limits formulated by FEMA 356 (2000) for the various earthquake levels considered in this experimental and numerical enquiry. The behaviour of the plastic hinges placed at the end sections of beams and columns was schematised by the constitutive laws also proposed in FEMA 356. In particular, yield rotations are expressed in this document by Eqs. (5-1) and (5-2), and resisting moments and interaction surfaces by Eqs. (5-3) and (5-4). Flexural hinges were assigned to beams, and coupled axial force-flexural moment hinges to columns. The generalized force-displacement relationship for all types of hinges, shown in Figure 10, was calibrated against the post-elastic parameters *a*, *b* and *c* suggested in Tables 5-6 and 5-7.

Peak interstory drift ratios and base shears referred to the eight selected tests summed up in Tables 4 through 7 are reported in Tables 8 and 9 for the original structure, as derived from the numerical enquiry, and in protected conditions, as drawn from the experiments.

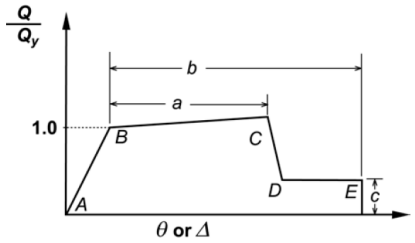

Figure 10. Generalized force-deformation relationship adopted for the definition of the behavioural characteristics of plastic hinges.

Table 8. Peak interstory drift ratio: comparison of response in original and protected conditions.

		Peak interstory drift ratio (%)			
		Story 1		Story 2	
Test	Ground motion	Prot.	Orig.	Prot.	Orig.
14	S1@PGA100%	0.09	0.94	0.12	1.18
15	S2@PGA100%	0.21	1.08	0.18	1.30
16	S3@PGA100%	0.36	1.23	0.36	1.41
20	S1@PGA150%	0.18	1.43	0.14	1.53
21	S2@PGA150%	0.36	1.60	0.30	1.57
22	S3@PGA150%	0.62	2.14	0.57	1.79
23	S4@PGA100%	0.34	1.01	0.30	1.23
34	S9@PGA125%	0.29	1.19	0.27	1.50

Table 8. Peak interstory drift ratio: comparison of response in original and protected conditions.

		Peak base shear (kN)	
Test	Ground motion	Prot.	Orig.
14	S1@PGA100%	37	143
15	S2@PGA100%	60	156
16	S3@PGA100%	87	158
20	S1@PGA150%	58	164
21	S2@PGA150%	99	171
22	S3@PGA150%	149	185
23	S4@PGA100%	83	152
34	S9@PGA125%	59	164

Data in Tables 8 and 9 highlight the following mean reductions of the interstory drift ratio for the four natural input motions, in protected configuration: 77% at first story, and 82% at second story, for ground motions scaled at 100% of PGA; and 79% at first story, and 82% at second story, for 150% scaled earthquakes. The corresponding reductions for the S9 artificial accelerogram scaled at 125% of PGA are: 78% at first story, and 85% at second story. The drops in terms of base shear are: 58% for natural motions scaled at 100% of PGA, and 42% at 150% (mean values); and 64% for the artificial accelerogram.

The response in original and protected configuration was finally assessed by the procedure formulated in (Sorace and Terenzi 2008). The interstory drift ratio was adopted as the reference response parameter for this enquiry, and the evaluation was referred to the grid of performance levels defined in FEMA 356 (2000) for existing steel buildings. Five structural (S-1 – immediate occupancy; S-2 – damage control, S-3 – life safety, S-4 – limited safety, S-5 – collapse prevention) and five non-structural (N-A – operational, N-B – immediate occupancy, N-C – life safety, N-D – hazards reduced, N-E – not considered) levels and ranges were dealt with. Combination of these levels brings to twenty-five building performance levels (from 1-A, as resulting from the combination of S-1 with N-A, to S-5). According with the suggestions provided for steel frame structures in FEMA 356, the following interstory drift ratios were selected as the corresponding limitations: 0.7% – S-1; 1.5% – S-2; 2% – S-3; 3% – S-4 and >3% – S-5, for structural levels; and 0.3% – N-A; 0.5% – N-B; 1% – N-C; 2% – N-D and no limit – N-E, for non-structural levels. By crossing the two sets of values, the following limits for building performance levels were obtained (Sorace and Terenzi 2008): 0.3% – 1-A; 0.5% – 1-B; 0.7% – 1-C; 1% – 2-C, 1.5% – 2-D, 2% – 3-D; 3% – 4-E.

The assessment analysis was carried out assuming the S9 normative accelerogram as input, scaled at 50%, 100%, 125% and 150% of its original amplitude. The response data in protected conditions at 100% and 125% of PGA were available from the shaking table tests. These data were then integrated by four numerical analyses in unprotected conditions, for all the earthquake levels, and two additional numerical analyses in retrofitted configuration (at 50% and 150% of PGA). The representative points of the eight analyses are plotted in the earthquake level-interstory drift ratio diagrams in Figures 11 and 12, for the first and second story, respectively. The response points are compared in the two graphs with the building performance drift limits defined above, and generate the formal performance evaluation summed up in Tables 10 and 11.

A nearly stable reduction of drifts emerges from Figures 10 and 11 at the three highest hazard levels, equal to 78%, for the first story, and varying from 85% at 100% to 83% at 150% of PGA, for the second story. The drop reaches 85% (first story) and 92% (second story) for the action scaled at 50%. The drastic improvement of seismic performance warranted by the protection system is reflected by the attainment of the extreme capacity level 1-A at each hazard level,

for both stories, except for the first story at 150% of PGA, where the immediately lower level (1-B) is achieved. This corresponds to three (50% and 150%, first story; 50%, second story) up to four (100% and 125%, first story; 100%, 125% and 150%, second story) shifts of building performance through the accomplished retrofit intervention.

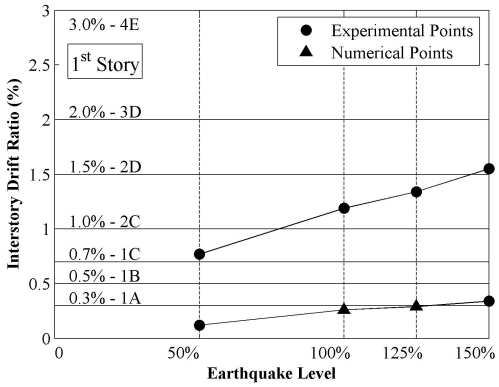

Figure 11. First story: interstory drift ratio as a function of the input ground motion level, and comparison with the assumed performance limitations.

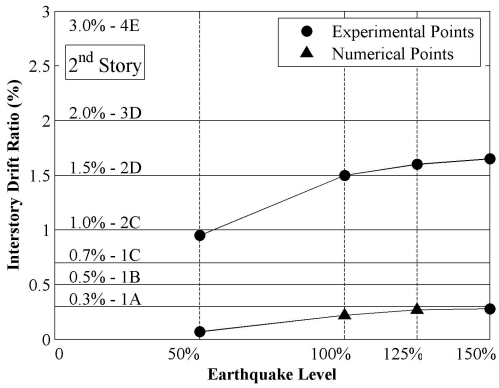

Figure 12. Second story: interstory drift ratio as a function of the input ground motion level, and comparison with the assumed performance limitations.

Table 10. First story: evaluated building performance levels.

Building performance level		
Earthquake level	Protected	Original
50%	1-A	1-C
100%	1-A	2-D
125%	1-A	2-D
150%	1-B	2-D

Table 11. Second story: evaluated building performance levels.

Building performance level		
Earthquake level	Protected	Original
50%	1-A	2-C
100%	1-A	2-D
125%	1-A	3-D
150%	1-A	3-D

ACKNOWLEDGEMENTS

The study reported in this paper was sponsored by the Italian Department of Civil Protection within the DPC-ReLUIS Executive Project 2005-2008. The authors gratefully acknowledge this financial support.

REFERENCES

CSI (2008). *SAP2000NL. Structural Analysis Programs*, Version No. 11.0, Computers & Structures Inc., Berkeley, CA.

Dolce M., Ponzo F. C., Cardone D., Di Cesare A., Ditommaso R., Moroni C., Nigro D., Serino G., Sorace S., Gattulli V., Occhiuzzi A., Vulcano A., Foti D. (2008). JET-PACS Project: joint experimental testing on passive and semiactive control systems. *14th World Conference on Earthquake Engineering*. Beijing, China, October 12-17, Paper No. 12-01-0183, CD-ROM.

FEMA (2000). *Prestandard and commentary for the seismic rehabilitation of buildings*, FEMA 356, Federal Emergency Management Agency, Washington DC.

Iervolino I., Maddaloni G., Cosenza E. (2007). Accelero-grammi naturali compatibili con le specifiche dell'OPCM 3431 per l'analisi sismica delle strutture. *XII Italian National Conference on Earthquake Engineering,* Pisa, Italy, June 10-14, CD-ROM.

IMPW – Italian Ministry of Public Works (2005). *Norme tecniche per il progetto, la valutazione e l'adeguamento sismico degli edifici*, OPCM 3431, Rome, Italy.

Jarret SL (2008). *Shock-control technologies*, URL http://www.introini.info.

Molina F. J., Sorace S., Terenzi G., Magonette G., Viaccoz B. (2004). Seismic tests on reinforced concrete and steel frames retrofitted with dissipative braces, *Earthquake Engineering and Structural Dynamics*, **33**(2), 1373-1394.

Pekcan G., Mander J. B., Chen S. S. (1995). The seismic response of a 1:3 scale model R.C. structure with elastomeric spring dampers, *Earthquake Spectra*, **11**(2), 249-267.

Sorace S., Terenzi G. (2001). Non-linear dynamic modelling and design procedure of FV spring-dampers for base isolation, *Engineering Structures*, **23**(12), 1556-1567.

Sorace S., Terenzi G. (2003). Large-scale experimental validation of a design procedure for damped braced steel structures. *STESSA 2003*. Naples, Italy, June 9-12, 657-662.

Sorace S., Terenzi G. (2008). Seismic protection of frame structures by fluid viscous damped braces, *Journal of Structural Engineering*, *ASCE*, **134**(1), 45-55.

Sorace S., Terenzi G. (2009). Fluid viscous damper-based seismic retrofit strategies of steel structures: general concepts and design applications, *Advanced Steel Construction*, **5**(2) (in print).

Sorace S., Terenzi G., Fadi F. (2009). *Shaking table tests amd modelling of JETPACS frame equipped with dissipative braces incorporating pressurized fluid viscous dampers*, JETPACS Report No. 4, Italian Department of Civil Protection, Rome, Italy.

Uang, C. M., Bertero, V. V. (1988). *Use of energy as a design criterion in earthquake-resistant design,* Report No. UCB-EERC 88/18, Berkeley, CA.